Journal of Materials Chemistry A

PAPER

View Article Online
View Journal | View Issue

Cite this: J. Mater. Chem. A, 2014, 2, 681

Proton transport behaviour and molecular dynamics in the guanidinium triflate solid and its mixtures with triflic acid

Haijin Zhu,[a] Usman ali Rana,[b] Vijayraghavan Ranganathan,[c] Liyu Jin,[d] Luke A. O'Dell,[a] Douglas R. MacFarlane[c] and Maria Forsyth*[a]

Knowledge of the proton transport behaviour in electrolyte materials is crucial for designing and developing novel solid electrolytes for electrochemical device applications such as fuel cells or batteries. In the present work, high proton conductivity (approximately 10^{-3} S cm^{-1}) was observed in the triflic acid (HTf) containing guanidinium triflate (GTf) composites. The proton transport mechanism in the composite was elucidated by comparing the diffusion coefficients obtained from NMR and conductivity measurements. Several orders of magnitude enhancement of conductivity is observed upon addition of HTf to the organic solid, and this appears to follow percolation behaviour with a percolation threshold of approximately 2% HTf. The data support a structural diffusion (or Grotthuss) mechanism of proton transport with a calculated Haven ratio significantly less than unity. ^{13}C SUPER and ^{14}N overtone NMR experiments were used to study the mobility and symmetry of the triflate anion and guanidinium cation respectively at a molecular level. The former experiment shows that the CF_3 group in the anion displays fast and isotropic motion at room temperature. In contrast to the high mobility of the anion group, the ^{14}N overtone experiments indicate that the guanidinium cation is static in both the pure and the acid-containing GTf samples at room temperature. It is anticipated that these solid-state NMR techniques may be also applied to other organic solid state electrolyte materials to achieve a better understanding of their transport mechanisms and molecular dynamics.

Received 23rd August 2013
Accepted 8th November 2013

DOI: 10.1039/c3ta13344c

www.rsc.org/MaterialsA

1. Introduction

Proton-conducting materials are currently attracting significant interest from both industry and academic circles because of their broad applications for low- and intermediate-temperature fuel cells, *i.e.*, proton exchange membrane fuel cells (PEMFCs), direct methanol fuel cells (DMFCs), phosphoric acid fuel cells (PAFCs), and alkaline fuel cells (AFCs).[1] Anhydrous solid-state proton-conducting electrolytes are highly desirable as they can avoid leakage and volatility issues that are commonly observed with the liquid electrolyte systems or systems that require solvents, such as water, to maintain their high ionic conductivity.

There have been some efforts dedicated to the development of proton-conducting solid-state electrolytes from polymer materials,[2,3] but unfortunately the conductivities of these polymer electrolytes are usually too low for most applications at room temperature and in the anhydrous state, and are also highly dependent on the temperature and/or relative humidity. Ceramic conductors such as perovskite-type oxides, *e.g.*, $SrCeO_3$ and $BaCeO_3$, have demonstrated high proton conductivity and significant stability at high temperature and in the anhydrous state.[4,5] However, these materials are of considerable disadvantage due to their brittle properties.

Protic ionic liquids (PILs) are a proton-conducting sub-class of the ionic liquid family and have attracted much attention as next-generation proton conductors for fuel cell applications due to their high ionic conductivity, high thermal stability, non-flammability and ability to be used under anhydrous conditions.[6] In many cases PILs display similar physico-chemical properties commonly observed for aprotic ILs.

Many families of ionic liquids display rotatory phases and/or plastic crystalline phases in their solid state.[7,8] These solid state cousins of ionic liquids represent a unique family of materials by exhibiting short-range disorder but maintaining their long-range ordered crystalline lattice structure. Rotator phases are those where one or more of the ions can rotate on its crystallographic site but without any significant translational motion.[9] The locally disordered structure in plastic crystals is also generally associated with rotational motion or reorientations of

[a]Institute for Frontier Materials and the ARC Centre of Excellence for Electromaterials Science, Deakin University, Geelong, VIC 3216, Australia. E-mail: mforsyth@deakin edu.au; Fax: +61-03-92446868; Tel: +61-03-92446818

[b]Sustainable Energy Technologies (SET) Center, College of Engineering, King Saud University, PO-BOX 800, Riyadh 11421, Kingdom of Saudi Arabia

[c]Department of Chemistry and the ARC Centre of Excellence for Electromaterials Science, Monash University, Clayton, VIC 3800, Australia

[d]Department of Materials Engineering and the ARC Centre of Excellence for Electromaterials Science, Monash University, Clayton, VIC 3800, Australia

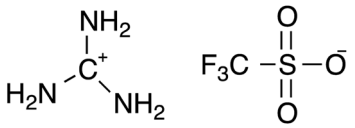

Fig. 1 Structural formula of guanidinium trifluoromethane sulfonate (GTf).

the molecules or ions.[10,11] As well as resulting in the plasticity of the materials, this local mobility is highly desirable because it is believed to result in the creation of vacancies[12] that facilitate fast ion transport in the materials. Whilst rotatory phases are important precursor phases for plastic crystals, they do not necessarily ensure plastic crystal behaviour or high intrinsic conductivity as will be seen for the pure material, guanidinium triflate, under investigation in the present work.

The guanidinium cation ($C(NH_2)_3^+$) is formed by protonation of the imine group on the basic guanidine molecule, with subsequent redistribution of the electron density of the double bond to yield three equivalent C–N bonds and a resonance stabilization of the whole entity as an ion with the three-fold rotational symmetry. It is relatively stable and can readily form ILs with stable anions such as triflate (Tf, $CF_3SO_3^-$), dicyanamide (DCA, $N(CN)_2^-$), thiocyanate (SCN^-), *etc.*[13] The six dissociable protons per cation make it an ideal candidate for a proton-conducting electrolyte. In our recent work, we have investigated the avenue of proton conductivity in the aprotic versions of organic ionic plastic crystals (OIPCs) by adding acids of various strengths and compositions.[14,15] High proton conductivity was achieved in the plastic crystal phase of various acid-containing OIPCs. In line with the emergence of these new proton-conducting materials, there is an increasingly urgent need to fully understand the nature and mechanisms of the ionic transport and related molecular dynamics in these materials. In the present work, we investigate the solid-state dynamics of a protic organic solid which we hypothesised may display OIPC behaviour, guanidinium triflate (Fig. 1), and its mixtures with triflic acid. It was initially hypothesised that diffusion of the additional proton from the doped acid would benefit from the six dissociable protons on the guanidinium cations, although we will show that this is not evident in this material despite achieving a very high conductivity with relatively low acid concentrations. The proton transport mechanism in the acid containing composites is therefore of particular interest in the present study. As we show, two advanced solid-state NMR methods provide us the possibility of probing the mobility and motional symmetry of the different ions in this novel material.

2. Experimental

2.1. Sample preparation

Guanidinium triflate (GTf) was synthesized by the reaction of triflic acid (HTf) with guanidinium carbonate. The synthesis of GTf involves the slow addition and stirring of 1 mole of aqueous triflic acid (7.2 g) to 1 mole of aqueous guanidinium carbonate (4.3 g) in a round bottom flask. During this reaction CO_2 was evolved and water was removed by distilling the reaction mixture at elevated temperature and reduced pressure. The solid product (yield 98%) was dried under vacuum. The acid doped samples were prepared by dissolving the doped amount of triflic acid in the GTf, homogenized by adding water and then using a rotary evaporator to remove the solvent, followed by further vacuum drying to remove any residual water. These samples are labelled as 'Doped' GTf samples, although we accept that this level of acid is significantly higher than usual doping levels. The neat material is a white powder, which easily forms into a rigid solid pellet upon pressing; whereas the doped samples were soft samples for which the pellets were readily deformed under pressure.

2.2. Differential scanning calorimetry (DSC)

DSC was performed on a TA-Q100 instrument. The samples were first heated up to 220 °C to completely eliminate any thermal history effects. Then the temperature was decreased to −100 °C at 10 °C min^{-1} and subsequently increased to 220 °C at 10 °C min^{-1}, and the phase transitions were recorded during the second heating scans.

2.3. AC impedance spectroscopy

The ionic conductivity was measured by the method of AC impedance spectroscopy using a Solartron® SI1260 impedance/gain phase analyser, which was connected to a Solartron® 1296 dielectric interface with the frequency range from 1 Hz to 1 MHz. A pair of gold coated stainless steel blocking electrodes was used to avoid the etching and oxidation from these acid containing materials. The whitish powder samples were pressed into pellets and then sandwiched between the electrodes for the conductivity measurement. All samples were packed and air-tightly sealed into a testing cell in a nitrogen atmosphere. Sample temperatures were controlled using a Eurotherm controller (model 2204), and measured with a type T thermal couple attached to one of the electrodes. The temperature was increased from 25 °C to 30 °C and then up to 140 °C with an interval of 10 °C. At each temperature, samples were equilibrated for 15 min before the impedance measurement was taken.

2.4. Cyclic voltammetry (CV)

CV experiments were carried out in a home-made Teflon three-electrode cell which consists of platinum working and counter electrodes and a silver quasi-reference electrode.[16] The measurements were carried out in an Ar filled dry box at 130 ± 2 °C with a scanning rate of 20 mV s^{-1} on a VMP2/Z potentiostat (Princeton Applied Research) under the control of EC-Lab V8.31 software. Samples were first ramped from room temperature to 130 ± 2 °C and were then equilibrated for 30 min before running the experiments.

2.5. Solid-state NMR

2.5.1. ^{1}H and ^{19}F static NMR experiments. All the ^{1}H and ^{19}F experiments were performed on a Bruker Avance III 300 MHz wide bore NMR spectrometer (^{1}H Larmor frequency of

300.13 MHz). A 4 mm double resonance Magic Angle Spinning (MAS) probe head was used to record the spectra from stationary powder samples. For both ^{1}H and ^{19}F experiments, the 90° pulse lengths were 2.5 μs, and the recycle delays were 30 s to allow the system to recover to equilibrium. The sample temperatures for the variable temperature experiments were calibrated with lead nitrate, using the method described in the literature.[17,18]

2.5.2. ^{13}C separation of undistorted powder patterns by effortless recoupling (SUPER) experiments. The SUPER experiments were performed on a Bruker Avance III 500 MHz wide bore NMR spectrometer. The basic principles and pulse sequence of SUPER experiments have been described elsewhere.[19] The ^{13}C nuclei were polarized by cross-polarization (CP) transfer from ^{19}F. A MAS rate of 4125 Hz and a scaling factor of 0.155 were used, resulting in an effective spectral width of 26.6 kHz for the indirect dimension, which is sufficiently large for the Chemical Shift Anisotropy (CSA) of the CF_3 group in the anion. The transmitter frequency was placed on-resonance with the signal from the CF_3 group. For the ^{13}C 2π recoupling pulses the $\omega_1 = 12.12\omega_r$ condition was satisfied by setting the power level to 50 kHz.[19] High powder ^{19}F decoupling was applied during the application of the ^{13}C 2π pulses.

2.5.3. ^{14}N overtone experiments. ^{14}N overtone MAS NMR spectra[20,21] were obtained at room temperature from the pure and doped samples on a Bruker Avance III 500 MHz wide bore NMR spectrometer (^{14}N overtone frequency of approximately 72 MHz) with a MAS rate of 12.5 kHz using a 4 mm double resonance probe. A WURST-80[22] excitation pulse of length 100 μs and a frequency sweep range of 120 kHz were generated using the Bruker Shapetool software. This pulse was applied at an RF power measured indirectly using the ^{1}H nuclei in D_2O, and corresponding to $\nu1(^{2}H) = 71$ kHz. Continuous-wave ^{1}H decoupling was also applied at a field strength of approximately 30 kHz. The spectra are referenced to twice the fundamental ^{14}N frequency in solid NH_4Cl, at 0 kHz. 1.2 million scans were acquired from each sample, with a recycle delay of 0.25 s.

Simulated overtone MAS powder patterns were generated using the Mathematica software and the Spindynamica code and fitted to the experimental spectra. Full details of these exact numerical simulations have been published elsewhere.[21] Simulations assumed a field strength of 11.7 T, a MAS rate 70 kHz and an ideal excitation pulse of 0.1 μs in length. 1154 crystallite orientations were used for powder averaging, calculated using the ZCW method. ^{14}N NMR parameters (quadrupolar coupling parameter C_Q, asymmetry parameter η_Q and isotropic chemical shift δ_{iso}) were adjusted until the simulated powder pattern matched the experimental spectrum. The simulated line was shifted down in frequency by twice the difference in the spinning rate to account for the fact that the $+2\omega_r$ overtone sideband was observed.[21]

2.5.4. ^{1}H and ^{19}F diffusion coefficient measurements. The HTf doped GTf samples were first sealed in a 4 mm solid-state NMR rotor, and then the rotor was inserted into a standard 5 mm glass tube for measurements. ^{1}H and ^{19}F NMR measurements were carried out on a Bruker Avance III 500 MHz wide bore spectrometer equipped with a 5 mm diff60 pulse-field gradient probe. The NMR signals of ^{1}H and ^{19}F of the doped HTf sample were used for the determination of diffusion coefficients (D_{H^+}, D_{Tf^-}) of the proton and anion species, respectively. The Pulsed Gradient Stimulated Echo (PGSTE) pulse sequence[23] was used to obtain the diffusion coefficient of different species. The diffusion coefficient, D^{NMR}, was calculated using the following equation:[24]

$$\ln\left(\frac{I}{I_0}\right) = -D^{NMR}\gamma^2\left(\Delta - \frac{\delta}{3}\right)\delta^2 g^2, \quad (1)$$

where I and I_0 are the signals in the presence and absence of the pulse-field gradient, respectively. γ is the gyromagnetic ratio of the nuclear studied. Δ is the interval between the gradient pulses, δ is the length of the gradient pulse, and g is the magnitude of the gradient pulse. In the present study, Δ was varied from 5 to 10 ms, δ was set between 1 and 4 ms, and g was optimized to a suitable gradient strength range from 0.3 to 29.4 T m^{-1} according to the diffusion coefficients. Recycle delays between were set to 5 s for all the diffusion experiments.

3. Results and discussion

3.1. Thermal properties and proton conductivity

As the molecular structure shows in Fig. 1, the guanidinium triflate contains six dissociable protons in each molecule, which would suggest it as a promising candidate for a proton conducting material. However, the crystallographic structure features a two-dimensional sheet of hydrogen between the six protons of each guanidinium cation and six triflate oxygen lone electron pairs from three neighbouring triflate anions.[25] Such extensive hydrogen bonding suggests that these protons may not be mobile enough to make GTf a good proton conducting electrolyte system. If an additional proton can be added *via* doping with acid, the acid proton may be able to either initiate proton migration *via* structural diffusion in the case of a solid solution phase, or diffuse through a grain boundary region in the case of a separated phase. This paper therefore aims to understand the molecular dynamics and proton conducting mechanisms of the guanidinium triflate system upon addition of triflic acid.

Thermal properties and phase transition behaviour are important because they have been shown to be closely related to the conductivity of solid-state crystalline materials.[7,26] The DSC melting endotherms of the pure GTf and 4 mol% HTf doped GTf samples are plotted in Fig. 2. The doped samples show a similar thermogram compared to the neat GTf sample. This suggests that the thermal properties of GTf are essentially unaffected by adding the acid. The melting point of both samples is about 160 °C, in agreement with the melting point of GTf that was reported previously.[13] A distinct solid–solid phase transition peak can be identified at a temperature of about 115 °C. Using the phase nomenclature suggested in the literature,[27] where the highest temperature phase is denoted as Phase I, the solid phases were labelled as Phase I and Phase II, respectively. The first solid–solid phase transition shows relatively low entropy change as compared to the melting. This may suggest that Phase I is structurally very similar to Phase II, and there may be an activated rotational motion and/or inter molecular

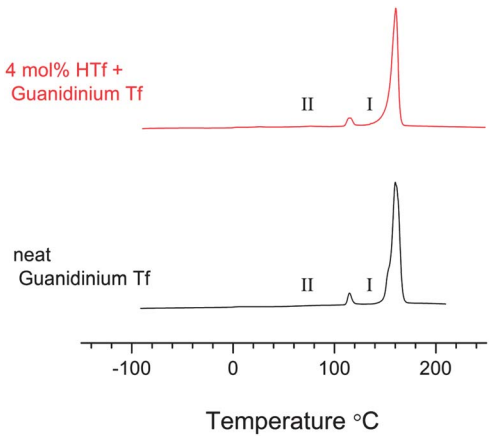

Fig. 2 DSC thermograms of the neat GTf and 4 mol% HTf doped GTf samples.

hydrogen bonding breakdown involved when the temperature goes through the solid–solid phase transition. Note that there is a suggestion of a low temperature shoulder at 160 °C in the neat system which may be an additional solid–solid phase transition which merges with melting.

The solid–solid phase transitions in plastic crystals are generally explained by the onset of rotational motions of particular parts of the molecules within a slightly expanded crystal lattice.[7,10,26,28,29] It is believed that activated rotational motions in the molecules which are responsible for the observed solid–solid phase transition can also be responsible for the increased ionic conductivity through the creation of vacancy and extended defects.[7,10] Fig. 3 shows the conductivity of the HTf doped GTf and that of the pure GTf samples measured in the temperature range of solid Phase II as identified from the DSC thermograms in Fig. 2. Both the pure GTf and 1 mol% doped samples show relatively low conductivity and strong temperature dependency. For the samples containing 2 mol% acid or more, the conductivities are very high, and surprisingly, relatively constant with increasing temperatures compared to those of the pure GTf and 1 mol% doped samples. The different temperature dependency of the 1 mol% acid sample and that of the higher content acid samples may hint at different proton conducting mechanisms. In order to further understand the proton transport mechanisms, the conductivities measured at 25 °C, 80 °C and 120 °C are plotted against the composition in Fig. 4. For all the measured temperatures, it is found that a dramatic increase in the conductivity, by several orders of magnitude, can be identified between the acid contents of 1–2 mol%. This behaviour is a strong indication of percolation-dominated conducting mechanisms in the system. Percolation theory deals with the effect of varying the number of interconnections presented in a random system.[30] In this case, the interconnections are the highly conductive HTf phase. Fournier *et al.* have proposed a model based on the Fermi–Dirac distribution which describes a critical non-conductor to conductor transition:[31]

$$\log(\sigma) = \log(\sigma_f) + \frac{\log(\sigma_m) - \log(\sigma_f)}{1 + \exp[b(p - p_c)]}, \quad (2)$$

where σ, σ_m, and σ_f are the conductivities of the composites, matrix and final composites, respectively. p is the mol percentage of the doped HTf, p_c is the percolation threshold concentration, and b is an empirical parameter that is related to the mechanisms which leads to the change of conductivity at the percolation threshold. Eqn (2) is fitted to the experimental data in Fig. 4. The best fit allowed the determination of the

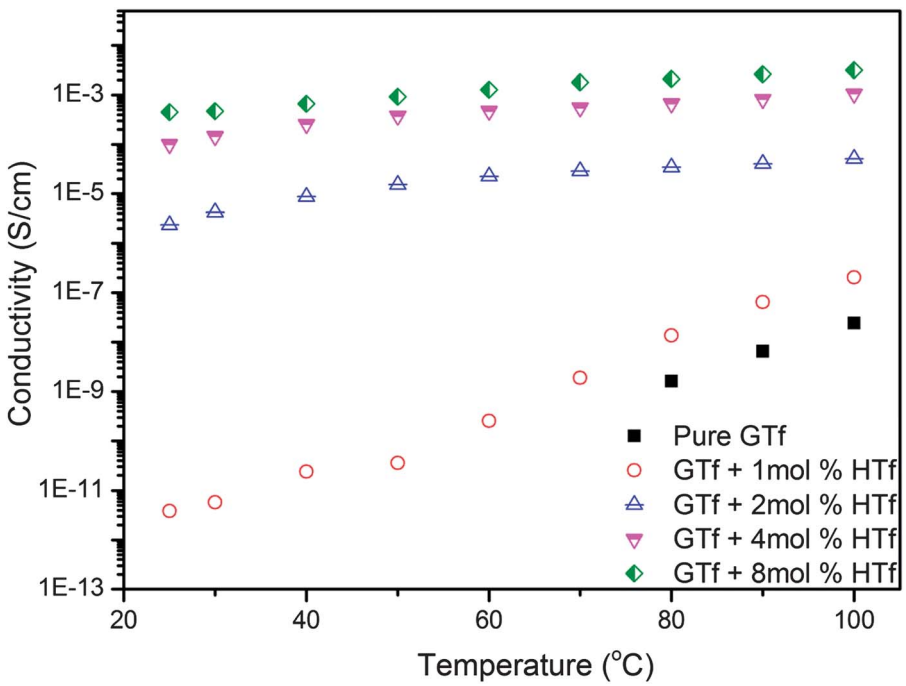

Fig. 3 Conductivity of the pure GTf salt and the doped GTf measured at different temperatures.

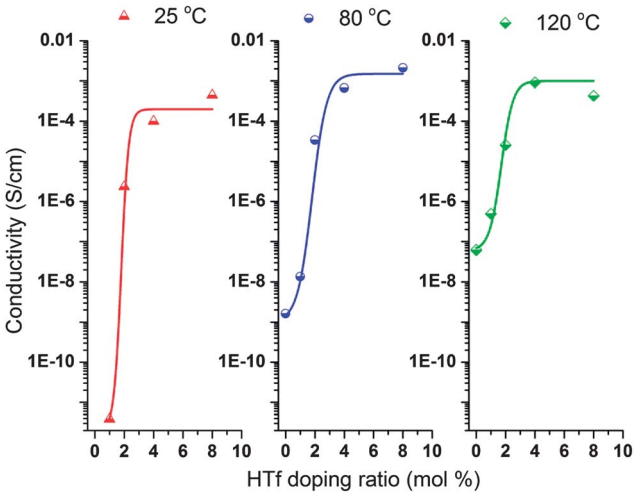

Fig. 4 Dependence of electrical conductivity of GTf composites on the mole fraction of HTf. The solid lines are the best fits to eqn (2).

percolation threshold (p_c) of the composites to be 1.8 mol%, 1.8 mol%, 1.7 mol% for the temperatures of 25 °C, 80 °C, and 120 °C, respectively. It can thus be seen that the percolation threshold remains essentially unchanged when the temperature increased from 25 °C up to 120 °C. This result strongly suggests that the percolation dominates the conductivity of the composites in the temperature range of 25 °C to 120 °C. Upon further increasing the temperature, the matrix also becomes conductive and contributes to the conductivity of the composites in addition to the percolation effect.

3.2. Proton reduction

The redox characteristics of the H^+ in the doped GTf sample were studied by using a cyclic voltammetry (CV) technique. The magnitude of the cathodic reduction current is an indication of the concentration and diffusivity of free protons present in the system. Fig. 5 shows the cyclic voltammograms of the pure and the HTf containing GTf samples. No H^+ reduction current was observed in the pure GTf sample even at elevated temperature (approximately 130 °C), despite the fact that there are 6 dissociable H^+ in the guanidinium cation which may be a rich H^+ reservoir. This result indicates that a low diffusivity of protons in the pure GTf sample is likely and this will be a bottle-neck for proton reduction even at high temperature. The HTf doped samples, however, clearly show rather high reduction currents (Fig. 5a and b). Moreover, the reduction current of the 8 mol% HTf sample is significantly higher than that of the 4 mol% HTf sample. The reasons for this enhancement in the reduction current are attributed to the increase of both the number of free H^+ and the diffusivity of the H^+ as will be discussed further in Section 3.4. During the reverse scans, the typical hydrogen oxidation reaction (HOR) was observed in the voltammograms of the acid containing samples. This property makes this system a favourable material for fuel cell applications.

3.3. Anion and cation mobility at ambient temperature

3.3.1. ^{1}H and ^{19}F mobility. As shown in Fig. 4, the addition of a low level (2 mol%) of HTf can already result in conductivity increases of several orders of magnitude. This phenomenon is attributed to the presence of fast H^+ ions in the composite. However, the question still remaining for discussion is how the fast H^+ ions interact with the low-conductivity GTf matrix in the composites. In previous work on different lithium doped [$C_n$mpyr][TFSA] OIPC systems, there has been some debate regarding the solubility of lithium salts and whether a true solid solution forms, or whether a eutectic forms whereby the added lithium salts form a mixture of phases with the OIPCs.[32–34] An investigation into the [C_1mpyr][I] system shows a significant increase in the mobility of the matrix cations upon doping with LiI.[35] This is the first direct evidence of a solid solution in the pyrrolidinium family. In the case of the GTf system, it is unclear how the molecular dynamics is affected by the additional H^+ from the HTf acid. Solid-state NMR has proven to be a robust analytical tool in assessing the mobility and interactions at a molecular level.[36,37] Both ^{1}H and ^{19}F are spin-half nuclei with nearly 100% natural abundance, and their static NMR spectra

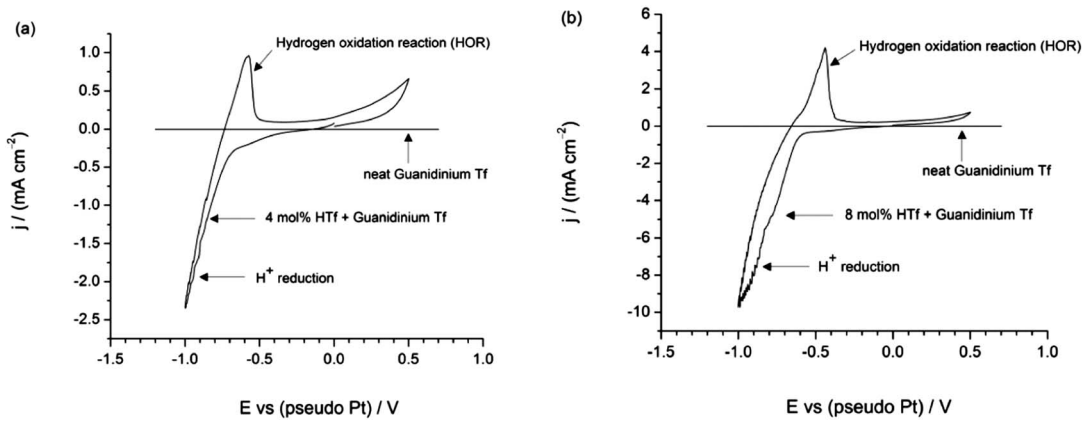

Fig. 5 Cyclic voltammograms of the (a) 4 mol% and (b) 8 mol% triflic acid and the pure GTf samples measured at 130 ± 2 °C. The voltammograms were obtained at a scan rate of 20 mV s^{-1} using bare Pt as a working electrode.

are therefore generally dominated by dipole–dipole interactions which result in broad and featureless peaks. However, the peak width can provide useful information about molecular motions, which may lead to line-narrowing.

As ^{1}H and ^{19}F solely exist in the cation and anion of these samples respectively, their NMR spectra allow us to probe the local dynamics of the individual species from an analysis of the linewidths. Fig. 6a shows a comparison of the ^{1}H NMR spectra of the pure GTf and HTf doped samples at room temperature. The spectrum of the pure GTf sample shows a characteristic shape known as a Pake doublet which is generally observed in a rigid system with strong ^{1}H dipolar couplings. The Pake doublet is composed of two subspectra resulting from the α and β spin states of two coupled nuclei. This means that the NH_2 protons in the pure GTf sample are strongly coupled with each other and that these groups are therefore not undergoing any fast dynamics (*e.g.*, rotation around the C–N bond). This is consistent with a previous crystallographic study which has shown extensive hydrogen bonding between the six protons of each guanidinium cation and six triflate oxygen lone electron pairs from three triflate anions at room temperature.[25] The spectrum of the HTf-containing sample is composed of a broad component with a narrow component superimposed. The narrow component is attributed to the fast H^+ from the HTf acid and the broad component is attributed to the protons in the GTf matrix. Comparing the lineshape of the two samples, one can easily see that the broad component of the 4 mol% HTf sample is essentially identical to the spectrum of the pure GTf sample. This means that the addition of HTf to the GTf matrix has no apparent effect on the ^{1}H local mobility of the GTf molecules at room temperature. This is a strong indication of phase separation in the system and implies that the added H^+ sits in the grain boundary and apparently has no access to the hydrogen bonded network in the GTf matrix.

In terms of the relationships between the microstructure and ionic transport behaviour, there are at least three mechanisms by which the doped anion and cation transport can affect the ionic conductivity of the composite: (I) the dopant anion and/or cation may intimately mix with the matrix and independently hop on the lattice vacancies or structural defects *via* structural diffusion; (II) the dopant may form an additional amorphous eutectic phase which is responsible for the high ionic conductivity of the composite; (III) the interactions between the dopant and the matrix are weak and thereby result in a heterogeneous grain boundary phase, which is rich in the additional component (in this case HTf). Mechanisms (I) and (II) require a good compatibility between the acid and matrix at a molecular level, and therefore it is expected that the molecular dynamics of at least some of the matrix ions would be modified upon adding the acid if the conductivity is dominated by either of these mechanisms, which is not the case for the present composite system. The results shown in Fig. 6 suggest that the conductivity in the grain boundary phase is the dominant mechanism responsible for the dramatic increase in the conductivity of the acid containing GTf samples.

The ^{19}F NMR spectra in Fig. 6b show similar results to the ^{1}H NMR spectra. The broad component of the HTf containing sample coincides with the spectrum of the pure GTf sample, which supports the argument that the HTf is located spatially in a different phase relative to the GTf matrix at room temperature, and therefore leaves the mobility of the anion group in the matrix unchanged. In order to further confirm this argument, the ^{1}H and ^{19}F spectra of the pure sample are subtracted from those of the doped samples and the difference spectra are shown at the bottom of each spectrum in Fig. 6. The concentration of mobile HTf estimated from the integrations of the ^{1}H and ^{19}F difference spectra over the original spectra of the GTf sample is approximately 4.5 mol% and 4.2 mol%, respectively. This result fits well with the experimental concentration for HTf of 4.0 mol%, within an experimental uncertainty. Some additional ions from the matrix would be expected to be contributing in the grain boundary phase which would also account for the slight increase in the mobile ion concentration.

3.3.2. Mobility of the anion and cation in the matrix. The previous discussion indicated that in the HTf–GTf mixtures studied here, the HTf component and the GTf matrix

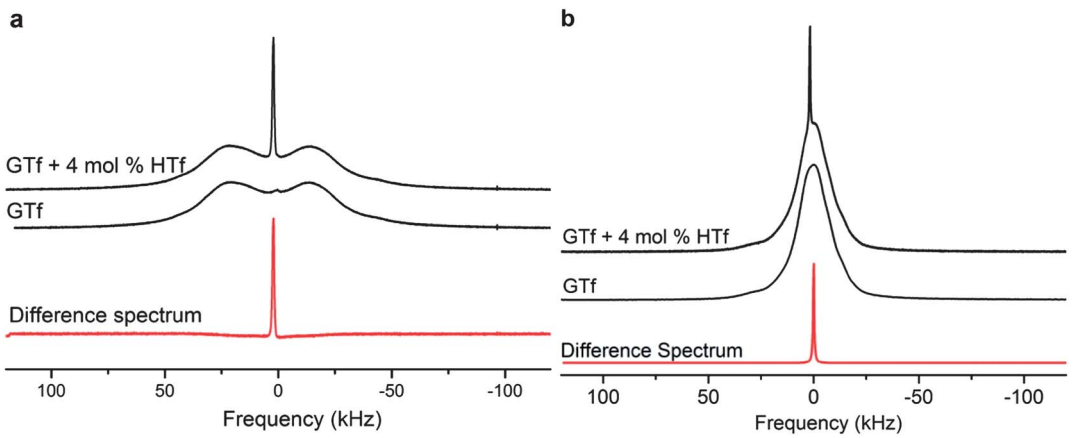

Fig. 6 The static ^{1}H (a) and ^{19}F (b) NMR spectra of the pure GTf and HTf doped GTf samples measured at 300 K. The difference spectra are shown as red lines at the bottom of each figure. T_1 of both ^{1}H and ^{19}F of both samples is roughly estimated to be less than 5 s. The recycle delays are 30 s for all measurements to allow the system to recover to equilibrium before the next excitation.

component have distinctly different molecular mobilities, as evidenced from the NMR spectroscopy. In the mixed system, both the added cation and anion groups are of high mobility, whereas the mobility of the anion and cation in the GTf matrix remains low and essentially unchanged compared to the pure GTf. This section aims to understand the local dynamics and motional symmetry of the anion and cation groups of both the pure GTf and the HTf containing samples. In solid-state NMR spectra, the chemical shift interaction can provide information on dynamics *via* chemical shift anisotropy (CSA), as well as information about the structure and symmetry of the molecules. Numerous techniques have been developed to reintroduce these interactions under magic angle spinning (MAS).[38] SUPER (Separation of Undistorted Powder Patterns by Effortless Recoupling) is one such experiment and can be used to obtain undistorted CSA powder patterns under MAS from nuclei such as ^{13}C.[19] The advantage of the SUPER experiment is the accurate measurement of the CSA symmetry parameters (η) at each ^{13}C site, which is sensitive to different dynamic modes. Fig. 7 shows the 2D ^{13}C spectrum obtained from GTf using the SUPER experiment. Only one ^{13}C peak can be observed in the spectrum which is assigned to the CF_3 group in the anion. Since the ^{13}C nuclei were excited *via* cross-polarisation from ^{19}F, the carbon site in the guanidinium cation group is not observed. Direct excitation was also unsuccessful for this site because of the high symmetry of the guanidinium ion which resulted in an extremely long T_1 relaxation time. Cross polarization from ^{1}H is also inefficient in polarizing this site because it is not directly bonded to any hydrogen nucleus.

The shape of the ^{13}C CSA pattern obtained in the $F1$ dimension of the SUPER experiment is a good indication of the motional symmetry of the anion in this case. If the molecules stay perfectly static, the three principle values of the chemical shift tensor determine the shape of the CSA pattern. As soon as molecular motions are involved, the shape of CSA pattern will be affected and the degree of perturbation is determined by the motional frequency as well as the geometry of the motion. Isotropic molecular reorientation usually averages the three principle values and gives an isotropic lineshape. The ^{13}C CSA pattern of the anion in the GTf sample shown in Fig. 7 lacks the characteristic features of a well-defined CSA powder pattern, and more closely resembles a broadened isotropic line. A possible explanation for this isotropic line shape might be due to the intrinsically symmetric environment which could lead to a small CSA. However, this is not likely to be the case for the present system considering the highly symmetric crystalline environment of the GTf salt, as shown by Russell *et al.*,[25] with $a = 12.99$ Å, $b = 7.5$ Å, $c = 18.45$ Å, $\beta = 111.69°$. Therefore, this isotropic line strongly suggests that the CF_3 group is not only rotating along the three-fold axis, but that the entire anion is also tumbling isotropically in space.

While experimentally very challenging, ^{14}N solid-state NMR spectra can also be a straightforward and informative probe for molecular structure and dynamics.[39] The difficulty of

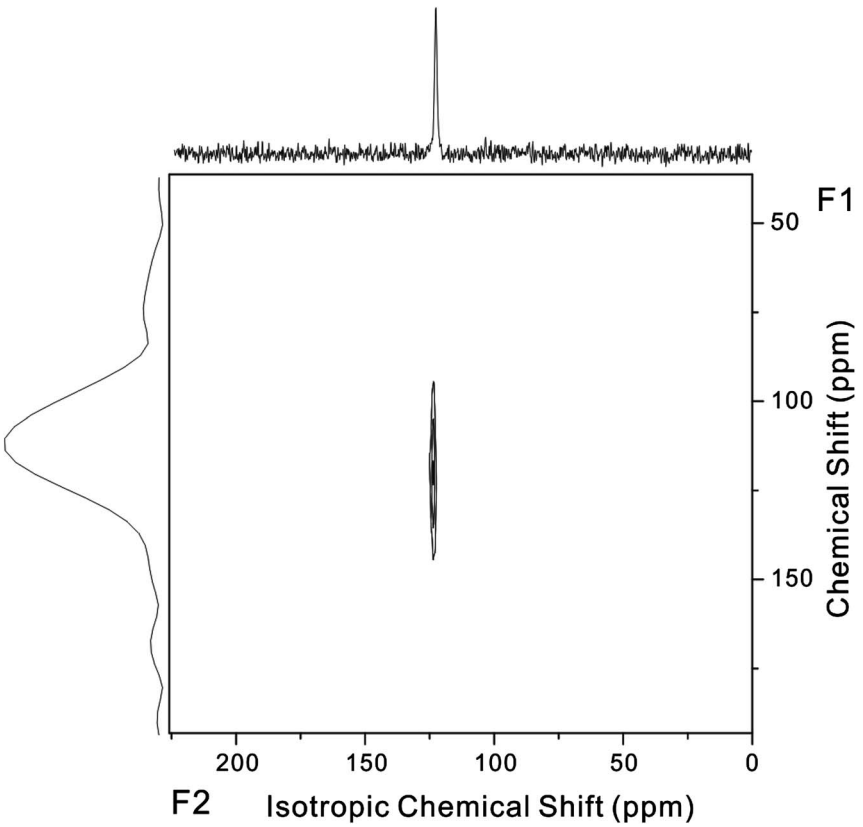

Fig. 7 ^{13}C SUPER spectrum of the pure GTf sample measured at 300 K.

^{14}N solid-state NMR arises from large perturbations to the Zeeman transitions due to the first-order quadrupolar interaction. ^{14}N overtone NMR is of particular interest because the first-order quadrupolar interaction which makes the fundamental transitions ($\Delta m = 1$) so difficult to study is absent. The overtone transition ($\Delta m = 1$) is only affected by the second-order quadrupolar transition, which is generally several orders of magnitude smaller than the first-order quadrupolar transition. Like the ^{13}C chemical shift anisotropy, this feature allows the dynamics of the guanidinium cation to be probed *via* the ^{14}N overtone pattern. The ^{14}N overtone MAS spectra obtained from the pure and doped GTf samples in Fig. 8 each show a single peak centred at around 85 kHz. The low sensitivity of the overtone signal is apparent in the figure with a relatively low signal-to-noise ratio for both spectra. However, the shape and position of the peak do provide useful information on the nitrogen environment within this sample. First, the position of the peak, which in this experiment is governed primarily by the second-order isotropic quadrupolar shift, is indicative of a quadrupolar coupling parameter of $C_Q = 3.3$ MHz, which is typical for a C–NH_2 nitrogen environment (*e.g.*, C_Q = 3.47 MHz for crystalline urea[39]). Secondly, the shape of the peak (quantified by the asymmetry parameter $\eta_Q = 0.9$) indicates a relatively asymmetric interaction tensor. This is expected given the asymmetric structure of the $C(NH_2)_3$ group, but it also rules out fast exchange of the sites that might result from three-fold reorientation of the guanidinium cation. Such a process occurring on a timescale of approximately 10^4 s^{-1} would result in a total loss of signal, while faster dynamics would lead to a motionally averaged and axially symmetric interaction tensor. This would both shift the position of the overtone MAS signal to a lower frequency and change its shape to a powder pattern featuring two sharp discontinuities.[21] These results therefore strongly indicate that the guanidinium cation is static in both samples at room temperature.

3.4. Diffusion and ionic conduction

The diffusion coefficient (D), also called diffusivity, is an important parameter indicative of the translational mobility of molecular species. One of the simplest techniques for the direct measurement of D is the Pulsed Gradient Stimulated Echo (PGSTE) NMR method.[23] It is worth noting that the diffusion coefficient measured by the PGSTE method consists of contributions from all the species including both the isolated and paired ions. This is in contrast to the diffusion coefficient calculated from the impedance spectroscopy method, *i.e.* measurements of AC conductivities, which only "see" the diffusion of charged particles (isolated ions). From the AC conductivity data, the DC conductivity, *i.e.* the limit for low frequencies, can be extracted. The Nernst–Einstein equation gives a direct relationship between ionic DC conductivity σ_{dc} and the ionic diffusion coefficient D^σ:

$$D^\sigma = \frac{\sigma_{dc} kT}{Nq^2}, \quad (3)$$

where $k = 1.3806505 \times 10^{-23}$ [J K^{-1}] is the Boltzmann constant, T [K] is the absolute temperature. N is the particle density of the charge carriers and q [C] is the charge of the ions. The diffusion coefficient D^σ obtained from conductivity is related to the diffusion coefficient which can be measured by NMR methods by the following equation:[40]

$$D^{NMR} = HD^\sigma, \quad (4)$$

where H is the Haven ratio which gives information about ion association. In the ideal case of completely dissociated single ions and random jumps, the diffusion coefficient D^{NMR} is identical to the ionic conductivity diffusion coefficient D^σ, and hence the Haven ratio $H = 1$. When correlations occur during the charge carrier transfer or when electronic conduction is also present, $H < 1$. When ionic association is present in the sample, such that diffusion is 'seen' by the NMR experiment but 'not seen' by the conductivity measurements (which only detects diffusion of charged species), one obtains $H > 1$.

The diffusion coefficients D^{NMR}, measured by NMR, and ionic diffusion coefficients D^σ, measured by AC impedance spectroscopy, are compared in Fig. 9. The D^{NMR} values of the anion group and proton ions in both samples are roughly constant within the measurement temperature range of 295 K to 343 K, whereas the ionic diffusion coefficients D^σ show an apparent temperature dependency for both samples. The D^{NMR} of $^1H^+$ and D_H^{NMR} values are approximately one order of magnitude higher than that of the anion group measured by D_F^{NMR}, for both 4 mol% and 8 mol% HTf samples. On one hand this can be understood in terms of the larger mass and size of the anion group compare to the $^1H^+$ but can also be linked to a correlated, structural diffusion for the H^+ ions compared with the vehicular motion of the anions. The D_H^{NMR} and the D_F^{NMR} values of the 8 mol% HTf sample are approximately 2 to 3 times and 3 to 7 times higher than that of the 4 mol% HTf sample, respectively. This molar ratio dependency of the diffusion coefficient of the anion and cation may suggest interfacial interactions between the doped HTf and the GTf matrix in the grain boundaries. The measured diffusion coefficient is a weighted average of the diffusion coefficient of the surface and bulk HTf molecules. The ion in HTf may be more restricted by the GTf surface at

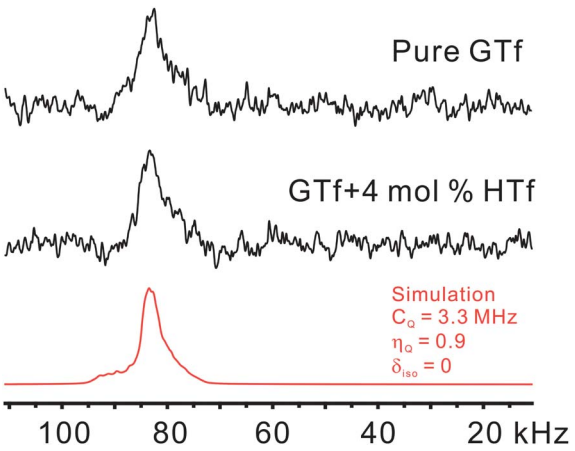

Fig. 8 ^{14}N overtone NMR MAS spectra of the pure GTf and 4 mol% HTf–GTf samples measured at room temperature.

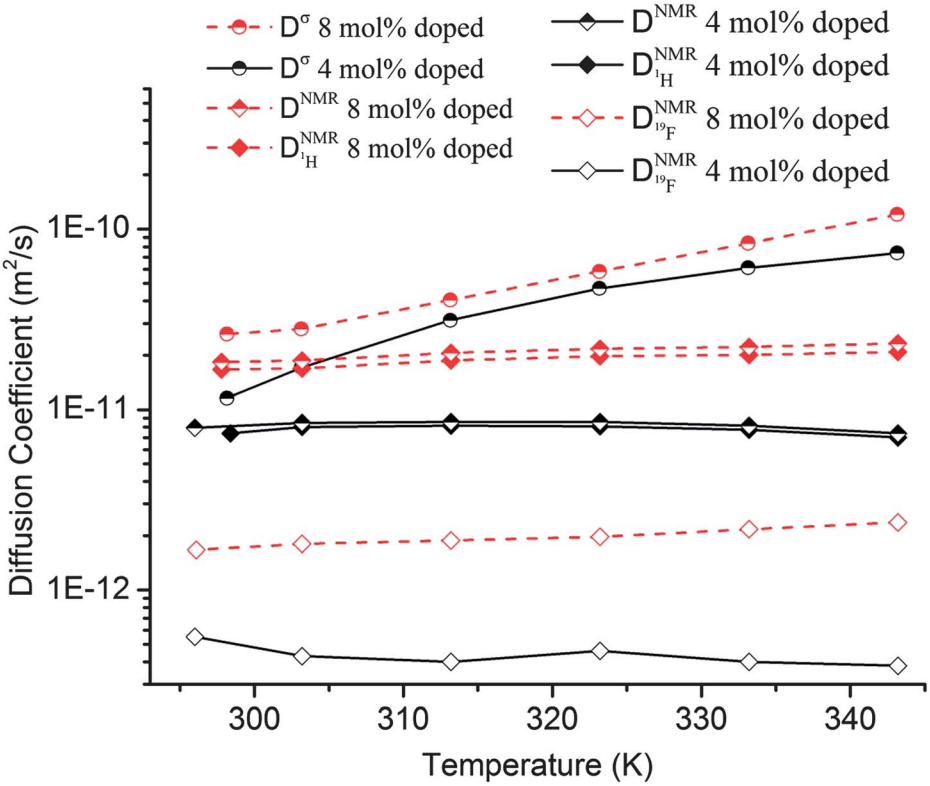

Fig. 9 Diffusion coefficient D^{NMR} and ionic diffusion coefficient D^{σ} at different temperatures measured by NMR and impedance spectroscopy, respectively. The D^{NMR} is a sum of D_H^{NMR} and D_F^{NMR}.

lower concentrations and therefore have lower diffusion coefficient than would be expected in the bulk HTf. As the molar ratio of the HTf increases, the relative fraction of the HTf interacting with the GTf surface at the grain boundaries decreases and so more of the HTf displays 'bulk' behaviour. This explains why the diffusion coefficients of both the anion and cation increase at higher HTf doping molar ratio.

Generally, the conductivity of a material consists of a superposition of the contribution of all charge carriers including anions, cations, electrons and holes. Therefore, the ionic diffusion coefficient calculated from the AC impedance includes contributions from both the anion and cation. To compare with the ionic diffusion coefficient D^{σ} obtained from the conductivity measurements, the diffusion coefficient of both the anion (D_F^{NMR}) and proton (D_H^{NMR}) is added together to give the overall diffusion coefficient (D^{NMR}) of the samples. The overall diffusion coefficient D^{NMR} values of both 4 mol% and 8 mol% HTf samples are plotted against the ionic conductivities D^{σ} at different temperatures in Fig. 10. The diagonal dashed line represents a line of Haven ratio $H = 1$. The upper-left part of the figure represents a region where $H > 1$, whereas the lower-right part represents a region where $H < 1$. It is observed that all the experimental points obtained at different temperatures for both the 4 mol% and 8 mol% samples are located in the region of $H < 1$. At lower temperatures, *i.e.*, 296 K, the Haven ratios of both samples are close to the line of $H = 1$; whereas at higher temperatures, the Haven ratio moves further away from the line of $H = 1$ in both cases. These results suggest that, first of all, in addition to the ionic conductivity of the anion and proton from the doped HTf, there are additional mechanisms that must contribute to the conductivity measured by AC impedance spectroscopy. One possibility is that there is an additional, growing contribution from the GTf matrix. On the other hand, at lower temperatures (296 K), the Haven ratio is close to 1, which suggests that the conductivity can be almost entirely explained by the individual diffusive contributions of the dissociated H^+ and Tf^- ions from the added HTf acid. With increasing temperatures the Haven ratio becomes smaller for both samples (as shown by the deviation of the data points from the dashed line at higher temperatures in Fig. 10). One explanation for this behaviour could be that the contribution to conductivity of the GTf matrix is increasing with temperature. This is also consistent with the conductivity data shown in Section 3.1 (Fig. 3 and 4), which shows significantly higher conductivity for the pure GTf sample at higher temperatures. On the other hand, $H < 1$ can also arise when there is a Grotthuss mechanism (also now known as structural diffusion[41,42]) of conduction involved wherein the addition by a hopping motion of a mobile proton to a hydrogen bonded network of acid molecules produces a proton shuffle through the network and results in the appearance of the added proton at some distant point, n hydrogen bonds away. In such a mechanism the NMR diffusion measurement detects the initial proton hop of about one hydrogen bond in distance whereas the conduction measurement detects a single charge appearing to move n hydrogen bonds in the same time interval. Thus an

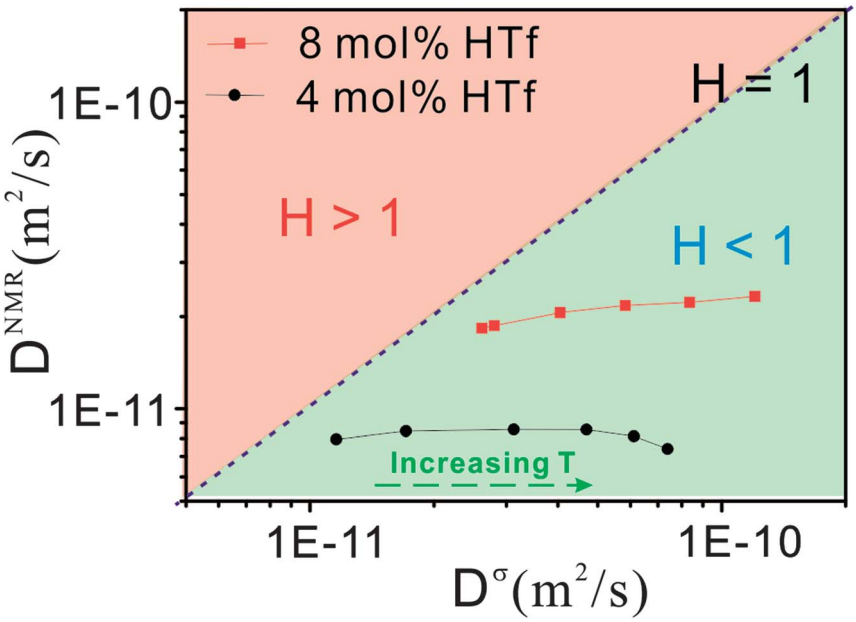

Fig. 10 Haven ratio of 4 mol% and 8 mol% GTf samples at different temperatures. The arrow at the bottom of the figure indicates the trend of the diffusion coefficients with change in temperature.

amplification of the proton motion is observed and the Haven ratio is decreased. This has been observed by Suarez *et al.* in superacids, although their definition of the Haven ratio in that case is inverse to what is typically defined in solid state conductors.[42] More detailed NMR correlation experiments at elevated temperatures would be useful in determining the relative contribution of these two mechanisms, however this is quite challenging at temperatures exceeding 100 °C.

4. Conclusions

This study aimed at understanding the molecular dynamics and the ionic transport behaviours in the HTf containing GTf system. The results of the conductivity measurements suggest that the high conductivity of these composites is dominated by a grain boundary percolation mechanism at room temperature. At higher temperatures, however, the GTf matrix also becomes conductive and likely contributes to the conductivity of the composites and therefore percolation theory fails in explaining the conducting mechanisms. This result is further supported by the diffusion experiments which show a Haven ratio of $H < 1$ as well as a decreasing Haven ratio with increasing temperature. Moreover, the HTf concentration dependency of the diffusion coefficient of the anion and proton may suggest interfacial interactions between the doped HTf and the GTf matrix. Solid-state ^{1}H and ^{19}F NMR lineshape analysis shows that the grain boundary conducting is the dominating mechanism which is responsible for the dramatic increase in the conductivity of the doped GTf samples at room temperature. The motional symmetry and molecular dynamics of the triflic anion and guanidinium cation were studied individually using ^{13}C SUPER and ^{14}N overtone NMR experiments. The ^{13}C SUPER results show that the triflic anion group displays a high rotational mobility. The CF_3 group is rotating along the three-fold axis, and the anion is also tumbling isotropically in space at room temperature. The ^{14}N overtone NMR experiments indicate that, on the other hand, the guanidinium cation is static in both the pure and the composite samples at room temperature. The Haven ratio being less than unity together with the significantly higher diffusion of the H^+ compared to the Tf^- anion also supports the idea of structural diffusion (or Grotthuss mechanism) transport for the H^+, most likely *via* hopping between the anions. This is in contrast to our original hypothesis where we expected the protons in the guanidinium matrix to assist in proton hopping; the NMR data clearly show that the guanidinium sublattice remains rigid up to the experimental temperatures achievable in this work.

Acknowledgements

MF and DRM are grateful to the Australian Research Council (ARC) for fellowship support under the Australian Laureate Fellowship scheme. The ARC is also acknowledged for funding Deakin University's Magnetic Resonance Facility through LIEF grant LE110100141. Dr Andreas Brinkmann (National Research Council, Canada) is thanked for writing the code to simulate ^{14}N overtone MAS spectra. SpinDynamica was programmed by Malcolm H. Levitt, Jyrki Rantaharju and Andreas Brinkmann, and is available at http://www.SpinDynamica.soton.ac.uk.

References

1 K.-D. Kreuer, S. J. Paddison, E. Spohr and M. Schuster, *Chem. Rev.*, 2004, **104**, 4637.
2 G. Alberti, M. Casciola, L. Massinelli and B. Bauer, *J. Membr. Sci.*, 2001, **185**, 73.

3 M. Rikukawa and K. Sanui, *Prog. Polym. Sci.*, 2000, **25**, 1463.
4 K. D. Kreuer, *Annu. Rev. Mater. Res.*, 2003, **33**, 333.
5 F. Lefebvre-Joud, G. Gauthier and J. Mougin, *J. Appl. Electrochem.*, 2009, **39**, 535.
6 M. A. B. H. Susan, A. Noda, S. Mitsushima and M. Watanabe, *Chem. Commun.*, 2003, 938.
7 L. Jin, K. M. Nairn, C. M. Forsyth, A. J. Seeber, D. R. MacFarlane, P. C. Howlett, M. Forsyth and J. M. Pringle, *J. Am. Chem. Soc.*, 2012, **134**, 9688.
8 J. M. Pringle, J. Golding, C. M. Forsyth, G. B. Deacon, M. Forsyth and D. R. MacFarlane, *J. Mater. Chem.*, 2002, **12**, 3475.
9 *Electrochemical Aspects of Ionic Liquids*, ed. H. Ohno, John Wiley & Sons, New Jersey, 2nd edn, 2011.
10 J. M. Pringle, P. C. Howlett, D. R. MacFarlane and M. Forsyth, *J. Mater. Chem.*, 2010, **20**, 2056.
11 D. R. MacFarlane and M. Forsyth, *Adv. Mater.*, 2001, **13**, 957.
12 J. N. Sherwood, *The Plastically crystalline state: orientationally disordered crystals*, Wiley, New York, 1979.
13 Z. Zhao, K. Ueno and C. A. Angell, *J. Phys. Chem. B*, 2011, **115**, 13467.
14 U. A. Rana, R. Vijayaraghavan, D. R. MacFarlane and M. Forsyth, *J. Mater. Chem.*, 2012, **22**, 2965.
15 U. A. Rana, R. Vijayaraghavan, D. R. MacFarlane and M. Forsyth, *Chem. Commun.*, 2011, **47**, 6401.
16 S. Long, P. C. Howlett, D. R. MacFarlane and M. Forsyth, *Solid State Ionics*, 2006, **177**, 647.
17 X. Guan and R. E. Stark, *Solid State Nucl. Magn. Reson.*, 2010, **38**, 74.
18 A. Bielecki and D. P. Burum, *J. Magn. Reson., Ser. A*, 1995, **116**, 215.
19 S. F. Liu, J. D. Mao and K. Schmidt-Rohr, *J. Magn. Reson.*, 2002, **155**, 15.
20 L. A. O'Dell and C. I. Ratcliffe, *Chem. Phys. Lett.*, 2011, **514**, 168.
21 L. A. O'Dell and A. Brinkmann, *J. Chem. Phys.*, 2013, **138**, 064201.
22 E. Kupče and R. Freeman, *J. Magn. Reson., Ser. A*, 1995, **115**, 273.
23 R. M. Cotts, M. J. R. Hoch, T. Sun and J. T. Markert, *J. Magn. Reson.*, 1989, **83**, 252.
24 J. E. Tanner and E. O. Stejskal, *J. Chem. Phys.*, 1968, **49**, 1768.
25 V. A. Russell, M. C. Etter and M. D. Ward, *J. Am. Chem. Soc.*, 1994, **116**, 1941.
26 D. R. MacFarlane, M. Forsyth, E. I. Izgorodina, A. P. Abbott, G. Annat and K. Fraser, *Phys. Chem. Chem. Phys.*, 2009, **11**, 4962.
27 J. M. Chezeau and J. H. Strange, *Phys. Rep.*, 1979, **53**, 1.
28 J. Golding, N. Hamid, D. R. MacFarlane, M. Forsyth, C. Forsyth, C. Collins and J. Huang, *Chem. Mater.*, 2001, **13**, 558.
29 K. J. Fraser, E. I. Izgorodina, M. Forsyth, J. L. Scott and D. R. MacFarlane, *Chem. Commun.*, 2007, 3817.
30 B. Bollobás and O. Riordan, *Percolation*, Cambridge University Press, 2006.
31 J. Fournier, G. Boiteux, G. Seytre and G. Marichy, *Synth. Met.*, 1997, **84**, 839.
32 D. R. MacFarlane, P. Meakin, N. Amini and M. Forsyth, *J. Phys.: Condens. Matter*, 2001, **13**, 8257.
33 S. J. Pas, J. Huang, M. Forsyth, D. R. MacFarlane and A. J. Hill, *J. Chem. Phys.*, 2005, **122**, 064704.
34 J. Huang, A. Hill, M. Forsyth, D. MacFarlane and A. Hollenkamp, *Solid State Ionics*, 2006, **177**, 2569.
35 J. Adebahr, A. J. Seeber, D. R. MacFarlane and M. Forsyth, *J. Phys. Chem. B*, 2005, **109**, 20087.
36 H. Yang, A. C. C. Esteves, H. Zhu, D. Wang and J. H. Xin, *Polymer*, 2012, **53**, 3577.
37 H. Zhu, R. Graf, G. Hou, Y. Zhao, D. Wang and H. W. Spiess, *Macromol. Chem. Phys.*, 2010, **211**, 1157.
38 A. E. Bennett, R. G. Griffin and S. Vega, *NMR basic Principles and Progress*, Springer, Berlin, 1994.
39 L. A. O'Dell, R. W. Schurko, K. J. Harris, J. Autschbach and C. I. Ratcliffe, *J. Am. Chem. Soc.*, 2010, **133**, 527.
40 G. E. Murch, *Solid State Ionics*, 1982, **7**, 177.
41 P. Heitjans and S. Indris, *J. Phys.: Condens. Matter*, 2003, **15**, R1257.
42 S. N. Suarez, J. R. P. Jayakody, S. G. Greenbaum, T. Zawodzinski and J. J. Fontanella, *J. Phys. Chem. B*, 2010, **114**, 8941.